Cross sections for the Ni, Cu, Zn(^{16,18}O, xn) reactions near the Coulomb barrier

R. L. Robinson, J. K. Bair, C. H. Johnson, P. H. Stelson, W. B. Dress, and C. M. Jones
Oak Ridge National Laboratory, Oak Ridge, Tennessee 37830*
(Received 1 September 1976)

Cross sections for neutron emitting reactions induced by ^{16,18}O bombardment of ^{58,60,61,62,64}Ni, ^{63,65}Cu, and ^{64,66,67,68,70}Zn targets have been measured for projectile energies between 36 and 55 MeV by means of a large graphite sphere with embedded $^{10}BF_3$ detectors. Comparisons were made with the total reaction cross section calculated with (1) the optical model, (2) the sharp cutoff model, and (3) the parabolic-barrier model. The data are generally in good agreement with the optical-model predictions above the Coulomb barrier if the neutrons are assumed to be emitted statistically from a compound nucleus and if fusion is the predominant mechanism. Interaction barriers obtained from the parabolic-barrier model yield interaction radii with values of (1.54 to 1.65)$(A_T^{1/3} + A_P^{1/3})$ fm.

[NUCLEAR REACTIONS ^{58,60,61,62,64}Ni, ^{63,65}Cu, ^{64,66,67,68,70}Zn(^{16,18}O, xn): $E = 36$–55 MeV. Measured total neutron yields.]

I. INTRODUCTION

The dependence of the total reaction cross section on projectile energy near the Coulomb barrier provides information on the height of the interaction barrier. A unique neutron detector system developed some 20 years ago by Macklin[1] has provided us with the capability to measure readily a cross section proportional to the total reaction cross section. This system, which basically is a large graphite sphere with embedded $^{10}BF_3$ detectors, has the virtues of high sensitivity and high absolute precision (cross sections with uncertainty of less than ±1% can be extracted under the best conditions). However, it has the drawbacks that it only detects reactions in which neutrons are emitted and its response is proportional to the number of neutrons emitted per reaction. Thus, for example, the cross section deduced for a reaction in which three neutrons are emitted would be three times the actual cross section.

We have determined cross sections for neutron-emitting reactions produced by bombarding ^{58,60,61,62,64}Ni, ^{63,65}Cu, and ^{64,66,67,68,70}Zn with ^{16,18}O projectiles with energies of 36 to 55 MeV (0.8 to 1.4 times the energy of the Coulomb barrier). The results have been compared with optical-model calculations. Systematic behavior of the energy of the interaction barrier was investigated with the sharp cutoff model and parabolic barrier model.

II. EXPERIMENTAL PROCEDURE AND RESULTS

Beams of ^{16}O and ^{18}O ions were provided by the ORNL EN tandem accelerator. The beam, after passing through two precision apertures—one of which, by monitoring the beam striking it, warned against improper beam alignment—impinged on a target located at the end of a 1-m-long Faraday cup. The target position was in the center of a 1.5-m-diam graphite sphere.[1] Neutrons thermalized by the graphite were detected by eight $^{10}BF_3$ detectors placed in the sphere. The graphite-sphere detector system was designed to have a flat neutron-energy response (within 1%) for neutrons with energies between 1 keV and 2 MeV. Above 2 MeV the response decreases with increasing energy. An experimental neutron spectrum had been measured[2] previously by the time-of-flight technique with a pulsed oxygen beam on a ^{58}Ni target and fitted with a nuclear temperature of 1.2 ± 0.1 MeV. These data and the known graphite sphere efficiency[1] were used to calculate a correction of (+3.7 ± 1.0)% to the measured yield from ^{58}Ni. This same correction was applied to data for all targets.

The absolute calibration of the detector was based on measurements made in June 1970 of the yield of the National Bureau of Standards NBS-II radium-γ-beryllium source. At that time a $\frac{1}{2}$-g radium source in a fabricated beryllium can was measured to serve as a local secondary standard. The absolute overall calibration constant is considered to be known[3] to ±0.6%. Also, measurements were made with a Pu-Be source which was used to check the detector efficiency from time to time during the experiment.

Target backings were platinum blanks that had been cleaned by scrubbing with an eraser, washing with solvents, and flaming to a red heat. The copper and nickel isotopes were prepared by vacuum evaporation of highly enriched separated isotopic metal. The isotopically enriched zinc targets were made by condensation of zinc vapor

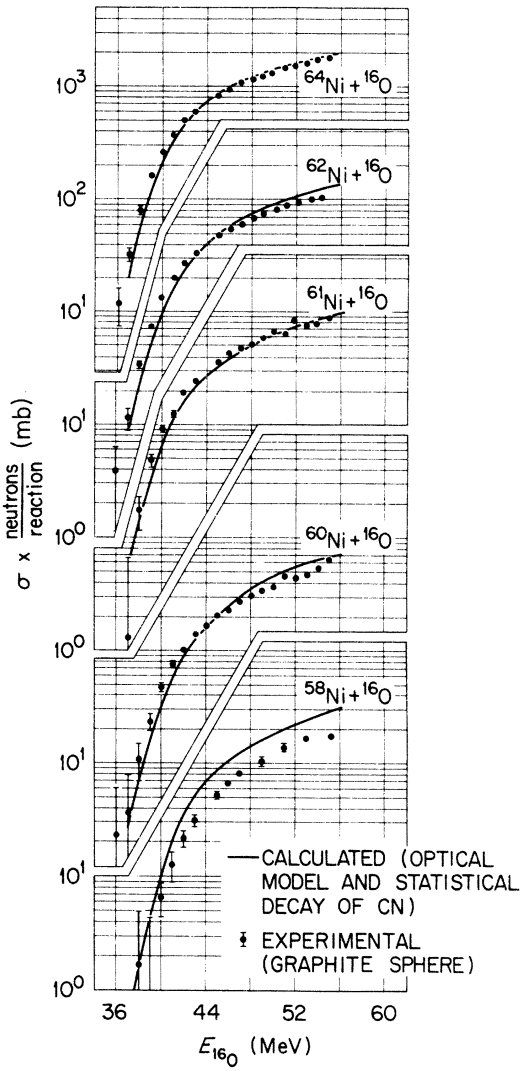

FIG. 1. Cross sections for neutron-emitting reactions resulting from the projectile and target noted in the figure. Experimental data are given by the points. Errors are shown when larger than the experimental point. Curves are products of the total reaction cross section calculated with an optical model and neutrons emitted per reaction calculated with a compound nucleus model.

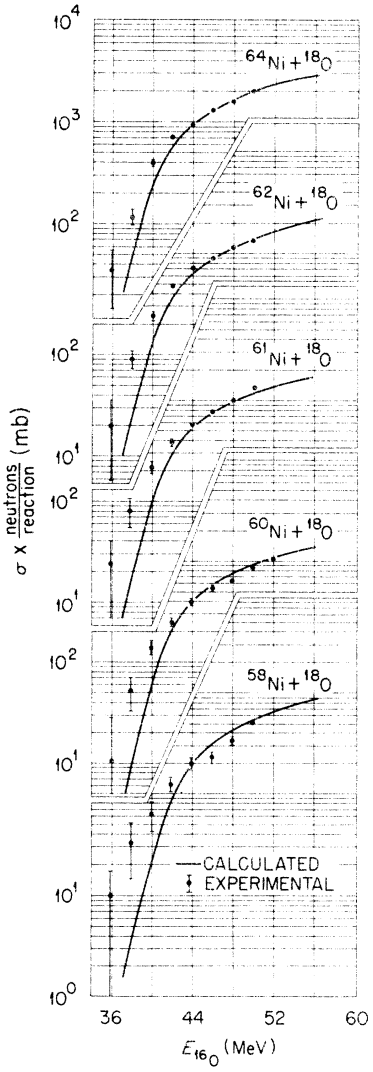

FIG. 2. See caption of Fig. 1.

at a high vapor pressure. Approximate target thicknesses were 50 to 90 μg/cm^2 for Ni, 100 μg/cm^2 for Cu, and 70 to 230 μg/cm^2 for Zn.

For many of the targets used in the course of this work, background measurements were made on the cleaned blanks before any target material had been deposited. After deposition it was found that the background yield at low energies had increased by a factor averaging about 3. More detailed measurements showed that this yield had the shape of that of carbon and/or oxygen as measured in an auxiliary experiment. Thus, in measuring a particular target, data were taken down to energies well below the barrier of the target material, and the known carbon and/or oxygen backgrounds were then fitted in this low-energy region to furnish the background to be subtracted at the higher energies. In general, the subtraction was straightforward.

Figures 1–5 summarize the experimental results. Plots are given as cross sections times neutrons per reaction since the neutrons emitted per reaction cannot be determined experimentally. All data have been corrected for the presence of the other isotopes. Bombarding energies have been corrected for target thickness. In addition to the error bars indicated in the figure there is a rms uncertainty of ±8% for the Ni data, ±4% for the Cu data, and ±7% for the Zn data.

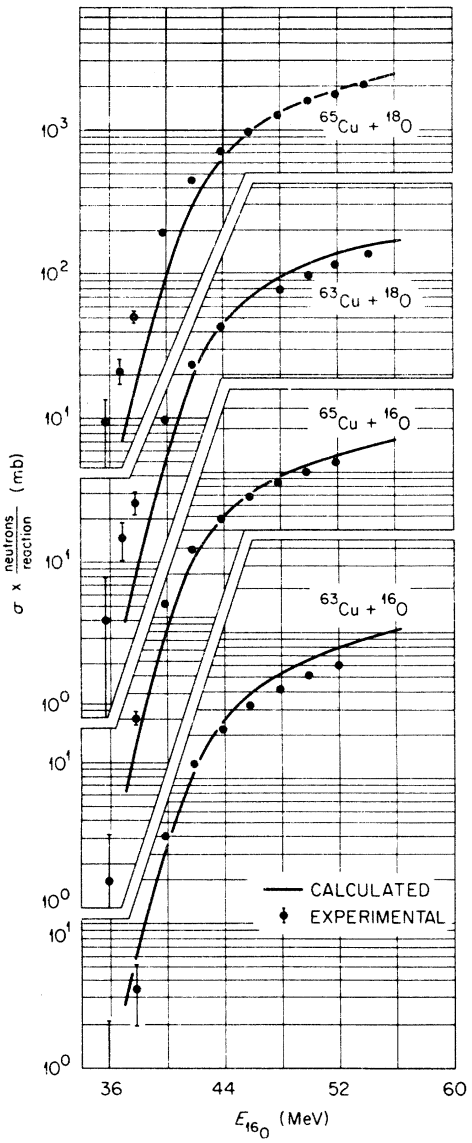

FIG. 3. See caption of Fig. 1.

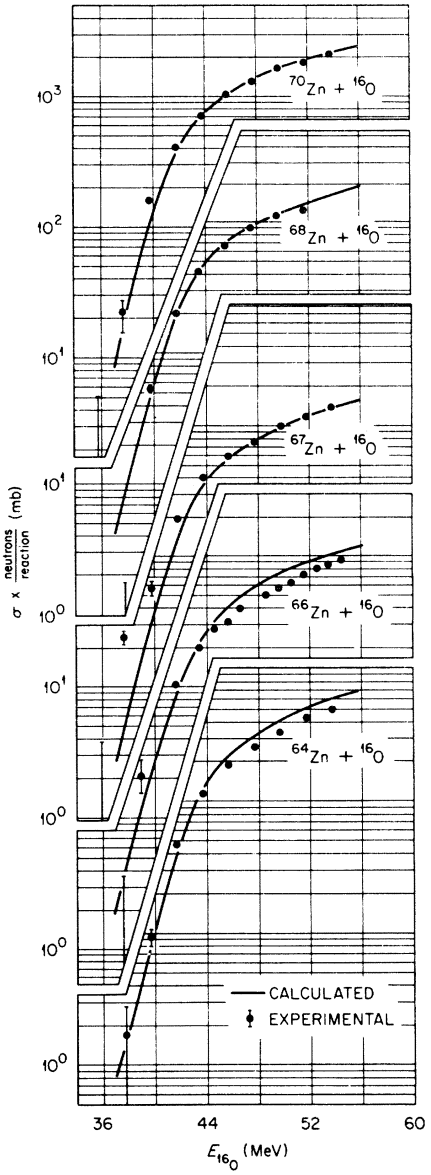

FIG. 4. See caption of Fig. 1.

III. DISCUSSION

In this section the results given in Figs. 1–5 are compared with several theoretical representations of the nuclear potential. In the first case, the total reaction cross sections were calculated with the optical model by means of the computer program GENOA.[4] In Refs. 5 and 6 it was shown that optical-model parameters reported by Christensen *et al.*[7] gave reasonable values for σ_R for ^{16}O on ^{58,60,61}Ni at energies above the Coulomb barrier. Their parameters were used here and are $V = 29.4$ MeV, $r_0 = r_0' = 1.30$ fm, $a = a' = 0.491$ fm, $W = 2.43$ MeV, and $r_{Coul} = 1.25$ fm. They were obtained from elastic scattering studies of ^{16}O on ^{58}Ni. However, these predicted reaction cross sections cannot be compared directly to our experimental results which only reflect channels in which neutrons are emitted and, furthermore, weight these channels by the number of neutrons emitted per reaction. To relate these two, we have used the compound nucleus computer program developed by Blann[8] and modified at Oak Ridge to include a subroutine written by Smith[9] which calculates transmission coefficients. This program BLANNTL calculates the cross sections for reactions produced by assuming the statistical probability for decay of the

compound nucleus and each resulting nucleus by proton, neutron, and α-particle emission until a level is reached in a nucleus which is stable to particle emission. Thus, with this program the neutron emission per reaction can be calculated. Figure 6 gives an example for the Ni + ^{16}O system as a function of projectile energy. As intuitively expected, neutron emission increases with increased neutron number in the target nucleus.

The product of the optical-model prediction for

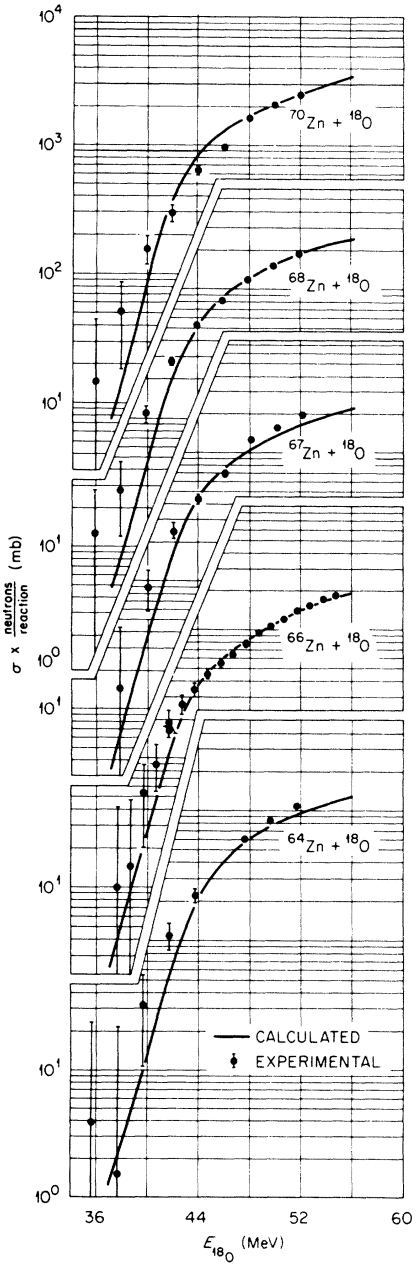

FIG. 5. See caption of Fig. 1.

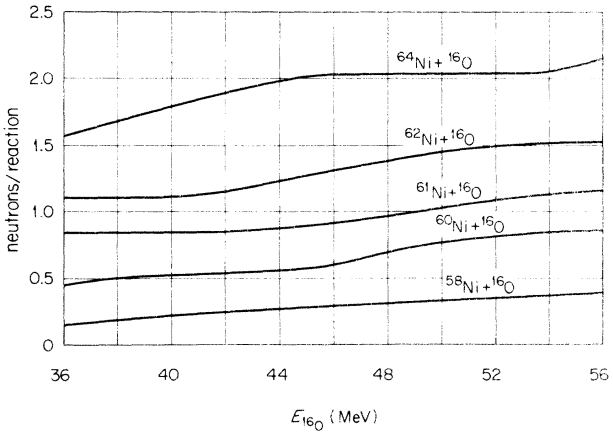

FIG. 6. Calculated average number of neutrons emitted per compound nucleus for reactions resulting from bombardment of Ni nuclei with ^{16}O ions.

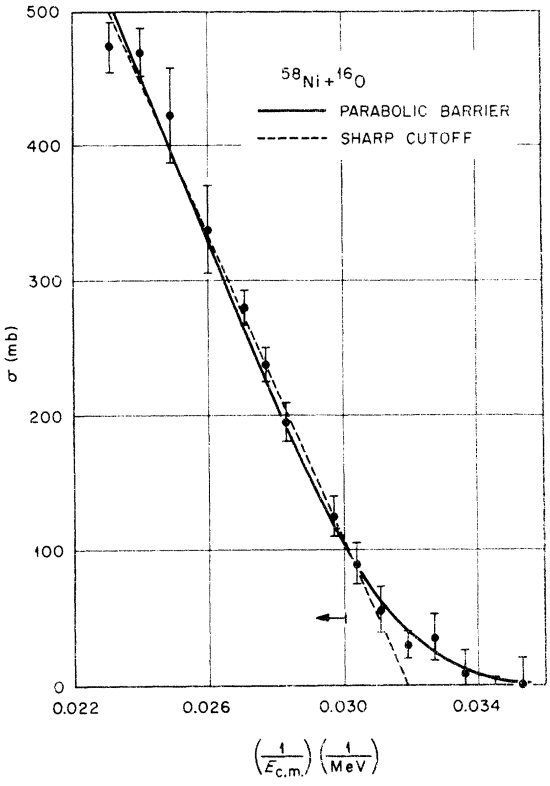

FIG. 7. Cross section vs $1/E_{c.m.}$ for the target and projectile noted in the figure. Points are experimental results divided by the calculated value for neutrons emitted per reaction. The dashed curve is predicted by the sharp cutoff model, and the solid curve is predicted by the parabolic barrier model. The dashed curve is fitted to the experimental points to the left of the arrow.

the total reaction cross section and the calculated neutrons per reaction is given in Figs. 1–5. With the exception of ^{58}Ni + ^{16}O predicted and experimental values agree at the higher projectile energies on average to about 5%. This suggests that for the projectile energies used in the present work most of the reaction cross section is due to fusion. It also indicates that the program BLANNTL for predicting products resulting from a compound nucleus reaction does a credible job for the stronger reaction channels.

The agreement between experiment and theory in Figs. 1–5 is not as good at the low projectile energies. Here theory is very sensitive to the choice of some optical-model parameters (see Ref. 5). Also note the agreement is worse for ^{18}O than ^{16}O. This fact may be because the optical-model parameters obtained for ^{16}O were used. The ^{58}Ni + ^{16}O data are in poor agreement with the calculated values for all energies. This reaction produces a compound nucleus which is farther from the valley of stability and emits fewer neutrons per reaction than any of the other projectile-target combinations considered. This poor agreement suggests that the model based on the statistical decay of particles from a compound nucleus and/or the assumptions incorporated into the BLANNTL program are not adequate for channels with small cross sections.

One of the more significant approximations of the BLANNTL program is that angular momentum is not included. To test the importance of this approximation, we calculated neutrons emitted per reaction for two cases, ^{58}Ni + ^{16}O and ^{62}Ni + ^{16}O, with a program which includes spin-dependent nuclear level densities and assumes neutrons, protons, and α particles carry off, respectively, two, three, and ten units of angular momentum.[10] The predicted cross sections were changed at most by 10% from those obtained with the program BLANNTL. Thus, this approximation alone cannot explain the difference in predicted and measured values for ^{58}Ni + ^{16}O.

A simple expression for the reaction cross section given by the sharp cutoff model is

$$\sigma_R = \pi R_f^2 \left(1 - \frac{V(R_f)}{E_{\text{c.m.}}}\right), \tag{1}$$

where R_f is the distance between the centers of the target and projectile at contact, and $V(R_f)$ is the potential energy at that radius. In this picture a plot of σ_R vs $(1/E_{\text{c.m.}})$ will be a straight line which intercepts the energy axis at $V(R_f)$. Several cases are plotted in this manner in Figs. 7–9. Our data have been corrected for the neutrons emitted per reaction as predicted by the program BLANNTL. The experimental results do fit a straight line, as can be seen in Figs. 7–9, except near the Coulomb barrier. Here there is deviation due to penetration of the barrier, an effect not accounted for by the simple expression in Eq. (1). The data for $E_{\text{proj}} \geq 43$ MeV, i.e., for energies where the deviation from a straight line in the σ vs $(1/E_{\text{c.m.}})$ plot is not perceptible, were least squares fitted to Eq. (1). The values of $V(R_f)$ extracted from this fit are listed in Table I. The errors reflect only

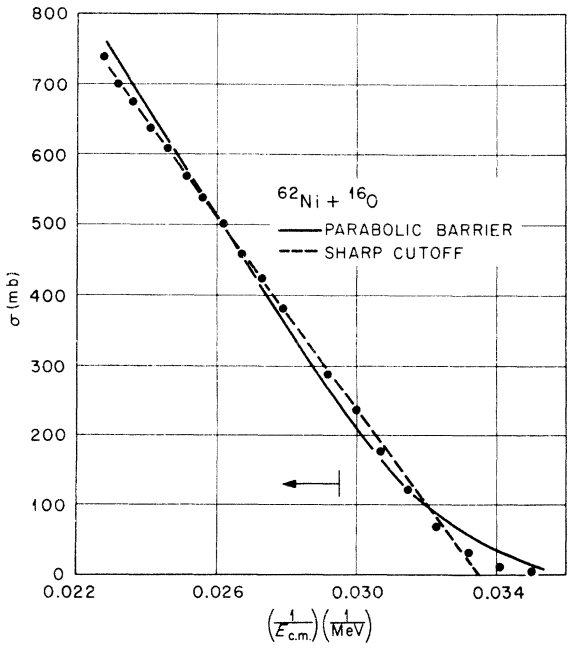

FIG. 8. See caption of Fig. 7.

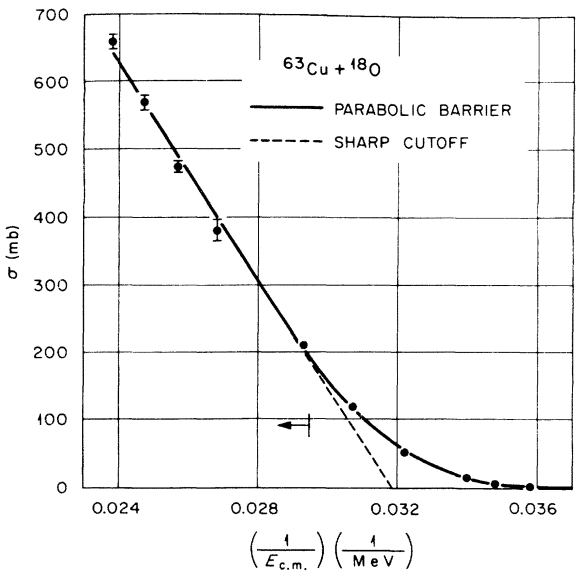

FIG. 9. See caption of Fig. 7.

TABLE I. Barrier heights obtained from comparison of experimental data with expressions in Eqs. (1) and (3).

Target	Sharp cutoff model $V(R_f)$ (MeV)	Sharp cutoff model r_{eff} (fm)	Parabolic barrier model V_0 (MeV)	Parabolic barrier model $(E_{\text{c.m.}}/V_0)$	Parabolic barrier model r_e (fm)
			^{16}O projectile		
^{58}Ni	31.4 ± 0.3	1.610 ± 0.015	31.6 ± 0.2	0.90 – 1.37	1.596 ± 0.010
^{60}Ni	29.5 ± 0.3	1.699 ± 0.017	30.4 ± 0.2	0.93 – 1.43	1.650 ± 0.010
^{61}Ni	30.4 ± 0.3	1.643 ± 0.017	30.9 ± 0.2	0.95 – 1.41	1.619 ± 0.010
^{62}Ni	29.9 ± 0.1	1.665 ± 0.006	30.5 ± 0.2	0.93 – 1.44	1.634 ± 0.010
^{64}Ni	30.8 ± 0.2	1.606 ± 0.010	30.7 ± 0.1	0.91 – 1.43	1.611 ± 0.005
^{63}Cu	31.0 ± 0.2	1.658 ± 0.011	31.9 ± 0.2	0.85 – 1.30	1.614 ± 0.010
^{65}Cu	30.9 ± 0.2	1.650 ± 0.011	31.7 ± 0.2	0.91 – 1.31	1.612 ± 0.010
^{64}Zn	32.5 ± 0.2	1.629 ± 0.011	33.1 ± 0.2	0.91 – 1.30	1.602 ± 0.010
^{66}Zn	32.6 ± 0.2	1.616 ± 0.010	32.7 ± 0.2	0.93 – 1.35	1.609 ± 0.010
^{67}Zn	32.3 ± 0.2	1.628 ± 0.010	32.6 ± 0.2	0.89 – 1.33	1.611 ± 0.010
^{68}Zn	32.6 ± 0.3	1.606 ± 0.015	33.2 ± 0.2	0.92 – 1.26	1.578 ± 0.010
^{70}Zn	32.1 ± 0.1	1.619 ± 0.007	32.5 ± 0.5	0.90 – 1.35	1.599 ± 0.010
			^{18}O projectile		
^{58}Ni	30.9 ± 0.8	1.608 ± 0.042	30.1 ± 0.5	0.86 – 1.27	1.650 ± 0.027
^{60}Ni	30.9 ± 0.5	1.596 ± 0.026	30.3 ± 0.3	0.91 – 1.32	1.627 ± 0.016
^{61}Ni	31.0 ± 0.5	1.587 ± 0.026	30.3 ± 0.3	0.91 – 1.27	1.624 ± 0.016
^{62}Ni	29.0 ± 0.3	1.691 ± 0.017	29.8 ± 0.2	0.88 – 1.30	1.644 ± 0.010
^{64}Ni	29.9 ± 0.3	1.629 ± 0.016	29.7 ± 0.2	0.89 – 1.31	1.638 ± 0.010
^{63}Cu	31.3 ± 0.3	1.617 ± 0.016	31.4 ± 0.1	0.84 – 1.34	1.614 ± 0.005
^{65}Cu	30.5 ± 0.3	1.647 ± 0.016	30.9 ± 0.1	0.86 – 1.37	1.628 ± 0.005
^{64}Zn	32.7 ± 0.4	1.596 ± 0.020	33.1 ± 0.2	0.84 – 1.22	1.578 ± 0.010
^{66}Zn	32.4 ± 0.4	1.601 ± 0.020	32.4 ± 0.3	0.91 – 1.33	1.599 ± 0.016
^{67}Zn	33.1 ± 0.4	1.561 ± 0.019	33.2 ± 0.3	0.90 – 1.24	1.555 ± 0.016
^{68}Zn	32.3 ± 0.4	1.595 ± 0.020	32.4 ± 0.1	0.87 – 1.26	1.593 ± 0.005
^{70}Zn	33.2 ± 0.4	1.542 ± 0.019	33.3 ± 0.2	0.86 – 1.19	1.538 ± 0.010

the uncertainty in the experimental points. Values of R_f were also determined from this fitting procedure. However, they depend as much on the predictions of the compound nucleus program as on the experimental data and thus are not included in the table. On the other hand, the values of $V(R_f)$ depend only weakly on the predictions of the compound nucleus program.

To remove the strong Z and A dependence from $V(R_f)$, we have calculated r_{eff} where

$$V(R_f) = \frac{Z_T Z_P e^2}{r_{\text{eff}}(A^{1/3}{}_T + A^{1/3}{}_P)} . \tag{2}$$

For a nucleus with a square-well potential, $r_{\text{eff}} = r_f = R_f/(A^{1/3}{}_T + A^{1/3}{}_P)$. For a more realistic potential, r_{eff} will be somewhat larger than r_f but will closely track changes in r_f.

The data were also least squares fitted to the expression

$$\sigma_R = \tfrac{1}{2}(R_0{}^2)\frac{\hbar\omega_0}{E_{\text{c.m.}}} \ln\{1 + \exp[2\pi(E_{\text{c.m.}} - V_0)/\hbar\omega_0]\} . \tag{3}$$

This expression was derived by Wong[11] assuming the nuclear potential near the barrier maximum is described by an inverted parabola. R_0, V_0, and $\hbar\omega_0$ are the radius, height, and curvature of the parabolic potential barrier for s waves. This model has been popular since it has a simple form and yet takes into account penetration of the nuclear potential. Vaz and Alexander[12] obtained the systematics of interaction barriers using this expression. However, they also included nuclear deformation effects by assuming that the interaction barrier has a uniform distribution of values between $V_0 - \Delta$ and $V_0 + \Delta$.

In fitting our data to Eq. (3) including the nuclear deformation, we first fixed $\hbar\omega_0 = 4.0$ MeV, an average value that Vaz and Alexander obtained from their fits of a large group of targets and projectiles. Then we took Δ, R_0, and V_0 as variables. However, for many cases the fitting procedure failed to converge (i.e., there are different sets of parameters which will fit the data). Since Vaz and Alexander chose $\Delta = 3.0$ MeV as an average value, we next fixed Δ at this value and varied

TABLE II. Average value for r_e for $^{16,18}O$ on each element.

Target	r_e (fm) ^{16}O projectile	^{18}O projectile
Ni	1.618 ± 0.009	1.637 ± 0.006
Cu	1.613 ± 0.007	1.621 ± 0.007
Zn	1.600 ± 0.006	1.581 ± 0.012

R_0 and V_0. Values of V_0 are given in Table I. Example fits are illustrated in Figs. 7–9. Column 5 in Table I shows the range of energies for the experimental points divided by the interaction barrier. Values of R_0 depend on the prediction of the compound nucleus program, as discussed for the sharp cutoff model, and are not given. The quantity r_e in Table I is obtained from V_0 by

$$V_0 = \frac{Z_T Z_P e^2}{r_e(A^{1/3}_T + A^{1/3}_P)} . \quad (4)$$

Table II gives a statistical average of r_e for a given element and projectile. This suggests that r_e decreases with increasing Z. Vaz and Alexander,[12] who fitted the reaction cross section for a wide variety of projectile-target combinations with the expressions in Eqs. (3) and (4), found r_e decreases approximately linearly with the $\ln(Z_T Z_P)$, although possibly not as rapidly as indicated by the results in Table II (see Fig. 14 in Ref. 12). For $Z_T Z_P = 224$ to 240, Vaz and Alexander's survey gives approximately 0.3% decrease in r_e; our results in Table II decrease by 2 ± 1%. The values in Table II are also above the visual curve drawn through the results in the paper of Vaz and Alexander. However, their curve is strongly influenced by cross sections obtained with proton and α projectiles. The present r_e's do appear consistent with just the heavy-ion results listed in their paper, and also with recent results of Scobel *et al.*[13] obtained by bombarding $^{58,60,62,64}Ni$ with ^{35}Cl. This can be seen in Fig. 10 which plots these values of r_e against $Z_T Z_P$.

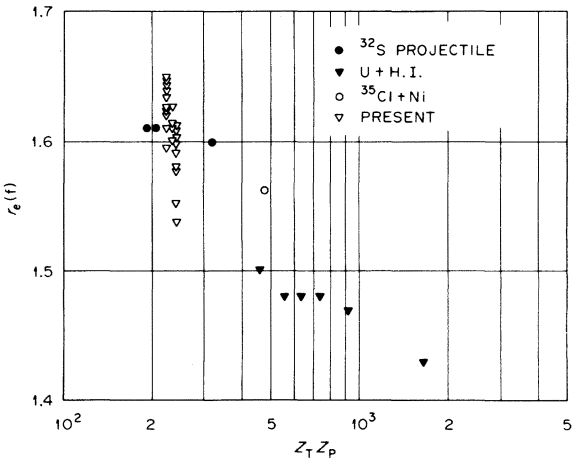

FIG. 10. Values extracted for r_e with the parabolic barrier model for heavy-ion induced reactions.

In summary, comparison of the measured and predicted cross sections indicates for the targets, projectiles, and projectile energies considered in this work, that the total reaction cross section is principally due to fusion followed by statistical evaporation of particles. From the shape of the measured cross sections as obtained near the Coulomb barrier, interaction barriers are extracted. Effective radii deduced from these are consistent with those found for other heavy-ion induced reactions.

*Operated by Union Carbide Corporation under contract with the U. S. Energy Research and Development Administration.

[1]R. L. Macklin, Nucl. Instrum. Methods 1, 335 (1957).
[2]H. J. Kim, P. H. Stelson, and R. L. Robinson (private communication).
[3]C. H. Johnson, J. K. Bair, C. M. Jones, S. K. Penny, and D. W. Smith (unpublished); J. K. Bair and H. M. Butler, Nucl. Tech. 19, 202 (1973).
[4]F. G. Perey (private communication).
[5]R. L. Robinson, H. J. Kim, and J. L. C. Ford, Jr., Phys. Rev. C 9, 1402 (1974).
[6]J. C. Wells, Jr., R. L. Robinson, H. J. Kim, and J. L. C. Ford, Jr., Phys. Rev. C 11, 879 (1975).
[7]P. R. Christensen, I. Chernov, E. E. Gross, R. Stokstad, and F. Videbaek, Nucl. Phys. A207, 433 (1973).
[8]M. Blann, in *Proceedings of the Heavy Ion Summer Study*, edited by S. T. Thornton (U.S. Atomic Energy Commission Technical Information Center, Oak Ridge, Tenn., 1972), Conf-720669, p. 269. Also, see discussion in Ref. 5 of the present paper.
[9]W. R. Smith, Comp. Phys. Commun. 1, 106 (1969).
[10]M. Blann and F. Plasil (private communication).
[11]C. Y. Wong, Phys. Rev. Lett. 31, 766 (1973).
[12]L. C. Vaz and J. M. Alexander, Phys. Rev. C 10, 464 (1974).
[13]W. Scobel, A. Mignerey, M. Blann, and H. H. Gutbrod, Phys. Rev. C 11, 1701 (1975).